Comparison of 7T 16-channel dual-row transmit arrays

M. Kozlov[1], J. Bode[1,4], P.-L. Bazin[1,5], N. Weiskopf[1], H.E. Möller[1], and G. Shajan[2,3]

***Abstract* – We evaluated and compared the performance of an inductively decoupled and overlapped dual-row transmit arrays for MRI at 7T. For the evaluated designs, the coupling between adjacent elements in the same row was higher for the overlapped compared to the non-overlapped configuration. However the transmit efficiencies for the circular polarization mode of both coils were similar. For comparisons of array transmit performance, consideration of array-internal losses as well as reflected and radiated power is very important, because their sum can be as high as 55% of the total transmit power.**

1 INTRODUCTION

One of the main challenges of ultra-high field (UHF, ≥7T) MRI is the spatially inhomogeneous distribution of the radio-frequency (RF) field resulting in an inhomogeneous signal distribution. Use of a transmit array coil offers increased flexibility to control and tailor the RF field distribution (RF shimming). Furthermore, extended longitudinal coverage and 3D RF shimming capability can be achieved by using multi-dimensional transmit arrays.

A number of factors are considered in selecting the transmit coil configuration. This includes transmit efficiency, SAR, coupling between the transmit elements, sample loading, distance between the coil and sample, RF shielding and integration of a multi-channel-receive array. In this study, RF transmit performance and S-parameters of two 16-channel dual-row transmit arrays are compared. The first configuration is the 7T version of [1] whereas in the second configuration, elements within the same row are geometrically decoupled.

2 METHOD

The first transmit coil (Fig. 1a) was constructed on a tube of 3 mm fiber glass with an inner diameter of 28 cm. It consists of 16 identical rectangular loops (100 mm × 102.25 mm) arranged in two rows of eight elements each. A gap of 10 mm was provided between the elements of the same row as well as between the two rows. The lower row elements were rotated by 22.5° with respect to the upper row. All adjacent elements were inductively decoupled.

The second transmit coil (Fig. 1b) was constructed on the tube of the same size. 16 identical rectangular loops (100 mm × 126.25 mm) were arranged in two rows of eight elements each. An overlap of 14 mm was provided between the elements of the same row. A gap of 10 mm was between the two rows. The lower row elements were rotated by 22.5° with respect to the upper row. The adjacent elements of different rows were inductively decoupled.

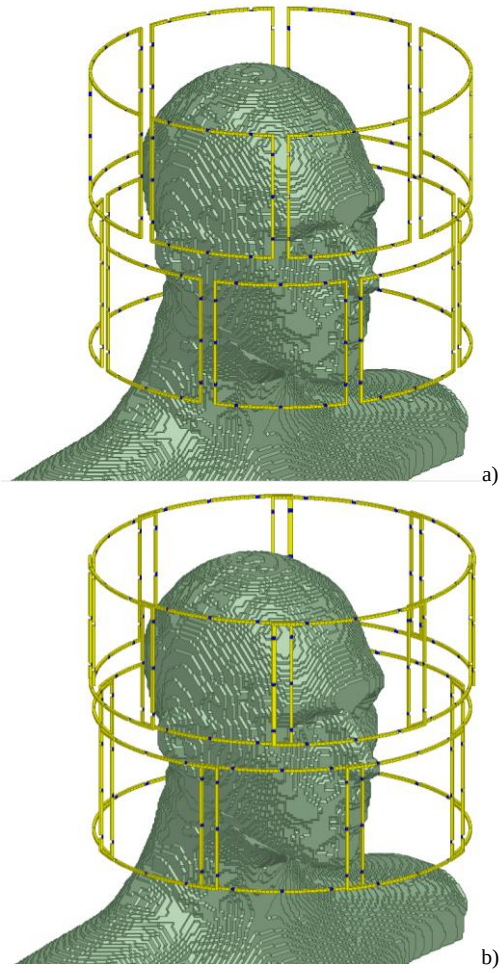

Figure 1: Array geometry setup: a) Non-overlapped design, b) Overlapped design. Only radiative elements and human model are shown.

12 distributed capacitors were placed in each radiative element, in positions shown as blue patches on the copper wire in Fig. 1, to provide feed, tune, shunt, and distributed capacitor functionality. One PIN diode, which was used for decoupling transmit-only radiative elements during MRI signal reception, with resistance 0.18 Ω was placed in series with one of the distributed capacitors.

The decoupling networks were defined by the inductors with inductance $L_{inductor}$ and coupling factor

[1] Max Planck Institute for Human Cognitive and Brain Sciences, Leipzig, 04103, Germany, e-mail: kozlov@cbs.mpg.de.
[2] Institute of Neuroscience and Psychology, University of Glasgow, UK: shajan.gunamony@glasgow.ac.uk.
[3] MR Coiltech Limited, UK.
[4] University of Applied Sciences Münster, Department of Engineering Physics, Münster, Germany
[5] Spinoza Centre for Neuroimaging, Amsterdam, the Netherlands

$K_{inductor}$, that were placed in series with the distributed capacitors. The Q factor of all capacitors was set equal to 324, and the Q factor of all inductors was set equal to 400.

Our investigation was performed using RF circuit and 3D EM co-simulation (Fig. 1) [2]. The RF circuit simulator was Agilent ADS 2016.01, while ANSYS HFSS 2014 was chosen as the 3D EM tool, for its robustness in handling complex coil geometry and fast multi-port simulation. The realistic 3D EM model of the array included a) all array construction details for the resonance elements, b) the load (e.g. surface based model of a phantom used for array performance validation), and c) array environment including MRI scanner gradient shield, magnet bore, all simulated with precise dimensions and material electrical properties. However, neither RF cable traps nor coax cable interconnection wiring were included in the model.

The tuning of the transmit array is based on the minimization of an error function (***EF***), which is a measure of the difference between the actual and desired array conditions ("optimization criteria"). Commonly used criteria for multi-channel RF transmitters, at the desired frequency, are: a) the element reflection coefficient $\boldsymbol{S}_{xx}$ must be set and equal to a required value (i.e., $\boldsymbol{S}_{xx\_t}$) for each array element; b) the element coupling $\boldsymbol{S}_{xy}$ must be equal to a required value (i.e, $\boldsymbol{S}_{xy\_t}$) for each decoupled element pair. Hence:

$$EF = \sum_{Elem} |S_{xx} - S_{xx\_t}|^2 + \sum_{all\_dec} 0.5 \cdot |S_{xy} - S_{xy\_t}|^2$$

where: *Elem* is number of loops of the coil (i.e. 16), *all_dec* is number of decoupled element pairs (i.e. 32 for non-overlapped and 16 for overlapped design).

To obtain a good match between numerical results and experiments, a phantom was scanned on a 3T whole-body scanner. The image resolution was 1.8×1.8×1.8 mm³ with a matrix of 257×194×242. The phantom image data was processed in MIPAV (ver. 7.3.0; https://mipav.cit.nih.gov), where the datatype was converted to boolean by thresholding. The image was cropped to cut lower parts of the model and get a flat bottom. The flat model boundary simplifies the model and reduces the memory necessary for 3D EM simulations, because all flat areas on one plane were merged to one surface object. It resulted in reduction of tetrahedral elements required to mesh the phantom. The tetrahedral mesh was generated via a marching cubes algorithm in ParaView (4.0.1 – http://www.paraview.org/). The resulting mesh consists of 259028 triangular elements. The zero covered boundaries lead to a closed surface. Without the padding there were holes in the mesh where the phantoms values touch the image boundaries. Further pre-processing of phantom model was done in HFSS.

3 RESULTS AND DISCUSSION

S parameters of the non-overlapped array are presented in Fig.2.

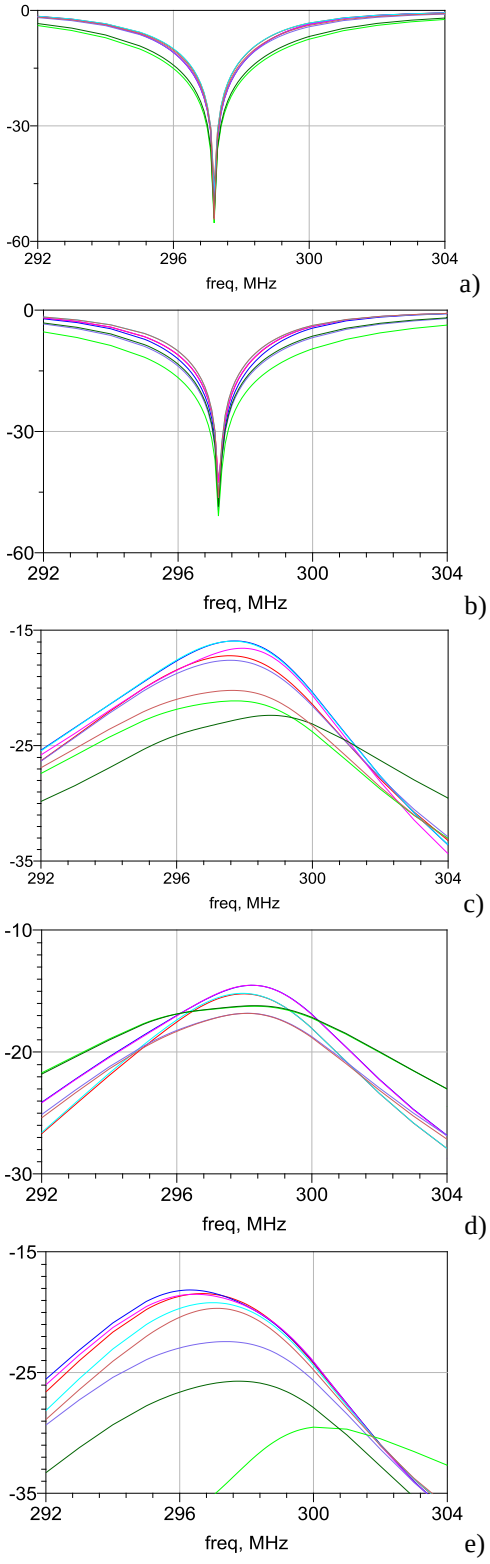

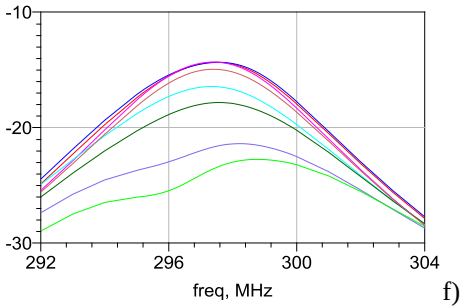

f)

Figure 2: Non-overlapped array: a) Sxx for the top row, b) Sxx for bottom row, c) Sxy for the top row, d) Sxy for the bottom row, e) Sxy between the inductively decoupled adjacent elements between the rows, f) Sxy between the nearest non-adjacent elements between the rows.

S parameters for overlapped array are presented in Fig.3.

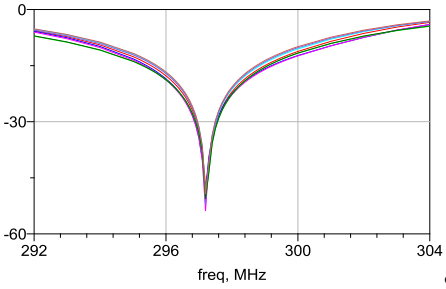

a)

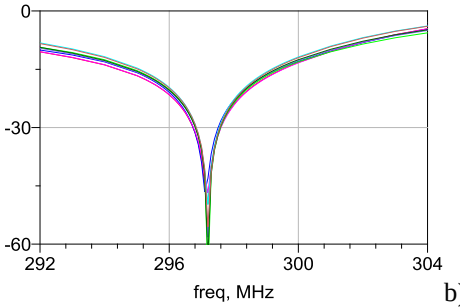

b)

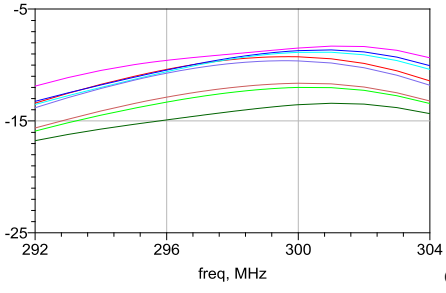

c)

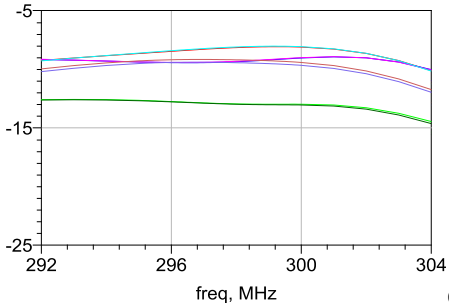

d)

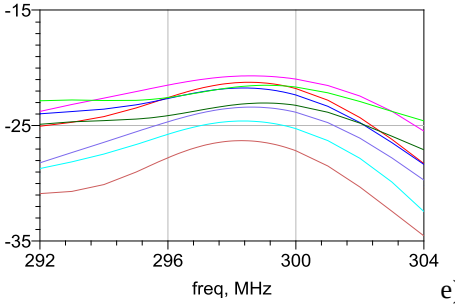

e)

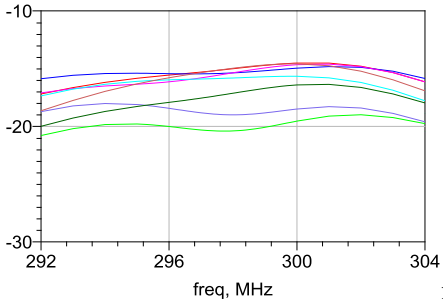

f)

Figure 3: Overlapped array: a) Sxx for the top row, b) Sxx for bottom row, c) Sxy for the top row, d) Sxy for the bottom row, e) Sxy between the inductively decoupled adjacent elements between the rows, f) Sxy between the nearest non-adjacent elements between the rows.

Power budget quantities and field results are presented in Table I.

TABLE I. POWER BUDGET AND SUMMARY OF FIELD RESULTS

	Non-overlapped	Over-lapped
Transmitted power, [W]	8	8
Reflected Power, [W]	1.13	2.11
Net Input Power, [W]	6.87	5.89
Radiated Power, [W]	1.44	1.23
Volume losses in all capacitors, [W]	1.02	0.68
Volume losses in all inductors, [W]	0.27	0.13
Volume losses in all pin-diodes, [W]	0.049	0.039
Resistive losses in conductors, [W]	0.11	0.09
Power deposition in the phantom, [W]	3.94	3.72
B1+ transmit coil center, uT	1.36	1.39
B1+ scanner iso-center, uT	1.47	1.50
B1+ phantom center, uT	1.43	1.44

Radiation losses of both coils were rather high. B1+ in the XZ plane is presented in Fig.4. The difference between field results of non-overlapped and overlapped arrays were negligible (Figs. 5 and 6).

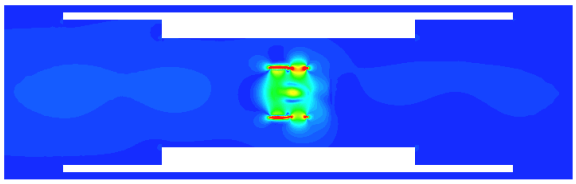

Figure 4: Non-overlapped array. B1+ in XZ plane.

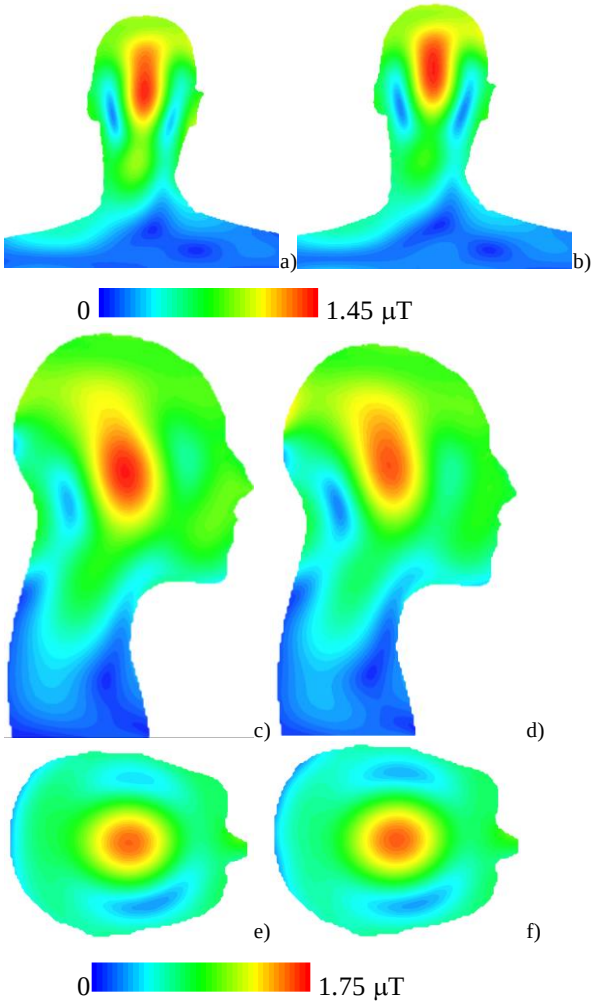

Figure 5: B1+ in µT for 8W transmit power. a), c), e) non-overlapped array; b), d), f) overlapped array.

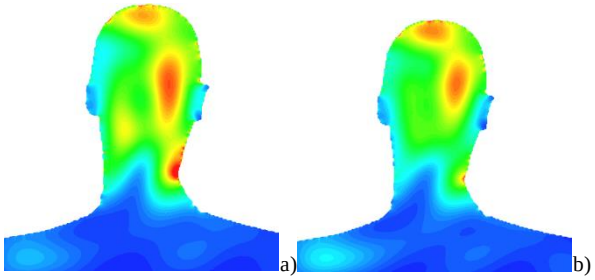

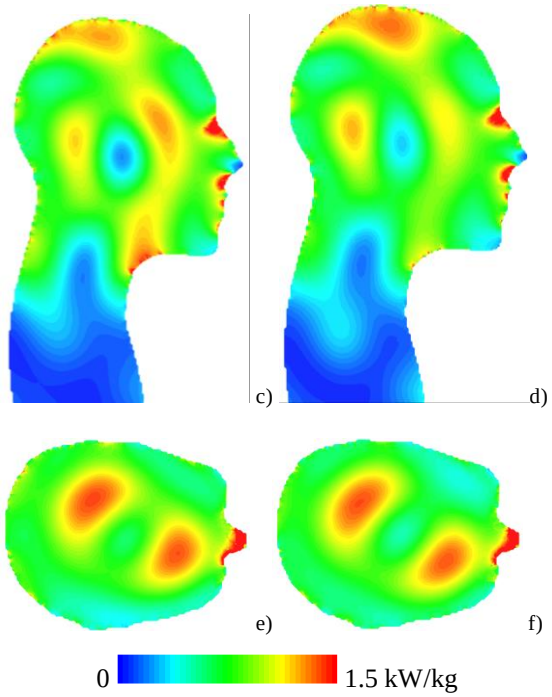

Figure 5: Volume loss density in kW/kg for 8W transmit power. a), c), e) non-overlapped array; b), d), f) overlapped array.

For selected overlap distances, coupling between adjacent elements in the same row was higher for the overlapped design. However the transmit efficiencies for circular polarization mode of both coils were similar. For comparisons of array transmit performance, consideration of array internal losses, reflected and radiated powers is very important, because their sum can be as much as 55% of the total transmit power.

The results derived from sophisticated static RF shimming optimization of arbitrary transmit amplitudes and phases, as well as calculation of transmit SENSE pulses and worst-case SAR analysis, should be performed before final decisions regarding coil configuration are made.

References

[1] G. Shajan, M. Kozlov, J.Hoffmann, R.Turner, K.Scheffler and R.Pohmann. A 16-channel dual-row transmit array in combination with a 31-element receive array for human brain imaging at 9.4T. Magn Reson Med 2014; 71:870-879.

[2] M. Kozlov, R. Turner, "Fast MRI coil analysis based on 3-D electromagnetic and RF circuit co-simulation," J. Magn. Reson., vol. 200, pp. 147-152, Sep. 2009.